Journal of Porous Materials
https://doi.org/10.1007/s10934-021-01161-6

Sulfated/Zr-containing mesoporous carbons: a promising nanostructured catalytic material

Oscar A. Anunziata[1] · **María L. Martínez**[1]

Accepted: 30 September 2021

Abstract
In this work, we report the successful preparation of a promising material with acidic properties from starch-derived mesoporous carbon (SMC), functionalized with sulfated zirconia (SZr-SMC). The process of assembling P123, starch, zirconia, and silicon produces ordered mesoporous carbon modified with Zr. Reaction time and temperature are essential to avoid the appearance of poorly assembled or unsightly structures, reducing the surface area and the size of the pores. SZr-SMC has a surface area of approximately 1300 m^2/g, and a total pore volume of 0.94 cm^3/g, composed mainly of mesoporous with an average pore size of 3.5 nm. The composition of the surface and the chemical states of the elements did not reveal ZrO_2 as isolated clusters. Ammonia thermodesorption studies indicated that, SZr-SMC retains 2.49 mmol/g of NH_3 at very high temperature, exhibiting a strong acidity. According to the data collected by infrared spectroscopy (FTIR), of pyridine desorbed at various temperatures, the total number of acidic sites was 2.36 mmol/g, and the distribution in weak- medium, strong, and super acidic sites was determined. The activity in the methylation of aniline and isopropanol dehydration indicated that the acid sites are strong, and have not redox properties. A new and promising catalytic material based on mesoporous carbons modified with sulfated Zr is developed, which opens a wide range of acid-catalyzed reactions applied to industrial and medical processes.

Keywords Sulfated-Zr-starch mesoporous carbon · SZr–C · SZr–O–C interactions · Super acidic properties

1 Introduction

Starch mesoporous carbon (SMC) has attracted attention as a new material due to its applications as drug carriers, catalyst support and energy storage medium [1]. Starch is a nontoxic and renewable carbon precursor and a natural polysaccharide compound; it is abundant and contains more than 49% of oxygen. High content of oxygen in starch results in the surface of starch-derived porous carbon with many hydrophilic groups, which can be widely functionalized in different applications. The carbohydrates available in biomasses are promising resources because they are the main source of natural carbon, renewable, and relatively economical [2]. Recently, heterogeneous acid catalysts such as sulfated zirconia [3] and tungsten zirconia [4], have been informed. The functionalization of Zr-SBA-15, with sulfonic groups in the catalyst, increases the acidity in the solid surface. Thus, Brönsted acid sites are found in a more available way, improving the selectivity to hydroxymethylfurfural (HMF), in the fructose dehydration [5]. Although all debate in the literature on the superacidity status and acid strength of sulfated zirconia, reports have confirmed that sulfated zirconia is truly a superacid, based on characterization results using Hammett indicators [6], and both pyridine (by FTIR) or ammonia (by TPD) [7]. In most of the works, the zirconia sulfate is found as a bulk of elevated dimensions, (several hundreds of nanometers, so looking for its decrease and thus greater surface area exposed and greater activity of the ZrO_2 crystals to be sulfated, Mishra et al. [8], attempted to nanonize them, reported crystals of sulfated zirconia around 25 nm. Although Zr-sulfate (SZr) has been widely used in industrial reactions, a few carbon-based sulfated zirconia supports have been reported [9–12]. It was recently informed that elevated acidity in sulfated zirconia supported over commercial activated carbon in the

✉ Oscar A. Anunziata
oanunziata@frc.utn.edu.ar

[1] Centro de Investigación en Nanociencia y Nanotecnología (NANOTEC), Facultad Regional Córdoba, Universidad Tecnológica Nacional, López y Cruz Roja Argentina, 5016 Córdoba, Argentina

Published online: 08 October 2021

synthesis of nitrogen heterocyclic compounds [13]. Budarin et al. [14], reported the synthesis of mesoporous coals called "starbons" using expanded mesoporous starch [15, 16], as a precursor without clathartic agent, exhibiting the use of starch's natural ability to form carbon-graphite structures with nanochannels. By varying the activation temperature, it was found that from 300to 600 °C aromatic systems arise, which then when heated to over 700 °C reach the carbon-graphite structure, being particularly suitable for use as catalysts. Carbon nanotubes are also candidates to be used as active species supports, due to their large surface area, thermal stability and tubular structure [17]. Dao-Jun Guo et al. [18], described a catalyst based on sulfated zirconia and supported by multiwall carbon nanotubes (MWCNT), which was found to contain high acidity, with nanoparticles layer coating on the MWCNT surfaces approximately 8 nm. Wan et al. [19], studied the synthesis of ordered mesoporous carbon and used it in the capture of CO_2 with high selectivity. Tan et al. [20], obtained mesoporous carbon as catalyst support for potential use in hydrodesulfurization reactions. These authors studied the NO chemisorption and observed that has a high NO uptake compared with commercial activated carbon. Superacid sulfated zirconium nanoparticles have been reported as potential chemotherapeutic active agents against neoplastic cells in the human colon and as an antimicrobial agent [21].

This research reports on our ongoing efforts to advance in the design of an acid catalyst based on carbon nanostructure. Thus, we developed a Zr-SMC-based acid catalyst functionalized with sulfated (SZr-SMC) with the typical carbon structure of graphite. The functionalization with sulfated Zr groups leads to the catalyst to exhibit super-acid properties and non-bulky ZrO_2 species. The goal of this work is the incorporation of zirconium, in the process of self-assembly of the template agents (P123) and hydrolyzed TEOS, and starch as a source of carbon in the original synthesis mixture. This direct incorporation of zirconia leads, after carbonization, to ordered mesoporous carbon material, with zirconium in its structure (Zr-SMC), and without zirconium oxide as a bulky species. The sulfated mesoporous carbon has a high acidity that can make the SZr-SMC material a catalyst with super acidic properties.

2 Materials and methods

2.1 Method of preparation

The synthesis of the materials was performed according to the related literature with further modifications [22]: starch (4.0 g), copolymer triblock, poly (ethyleneglycol)–poly (propyleneglycol)–poly (ethyleneglycol) (Pluronic P123, Sigma-Aldrich) 8.0 g and 320 mL HCl solution (2 M) was mixed in a Polypropylene bottle. The mixture was maintained at 35 °C in a water bath for 6 h under constant stirring. Then, 18.4 mL of tetraethyl orthosilicate (TEOS, 98%, Sigma-Aldrich) and Zirconium (IV) oxide chloride (99.99%, Aldrich) reaching to a solution with Si/Zr = 20 molar ratio. After stirring for 24 h, the solution was placed in an oven for 24 h at 100 °C without further stirring. The material previously washed was dried at 35 °C in a vacuum oven. The obtained precipitate (1 g) was then treated with 10 mL of deionized water and 98 wt% H_2SO_4 (1 mL), under stirring for 12 h, and pre-carbonized at 100 °C for 6 h. The pre-carbonized sample was calcined at 750 °C under nitrogen flow for 2 h. The resultant carbon/silica composite was washed with 40 wt. % HF solution to extract silica from the carbon framework. Finally, the material was washed with deionized water and successively dried, obtaining Zr-SMC material. Mesoporous carbon was functionalized with H_2SO_4 to become sulfated. The newly prepared material was called SZr-SMC, containing an atomic S/Zr ratio around 0.98($\pm$0.05) and total zirconia approximately 2.4 $\pm$ 0.05 mmol/g of the catalysts, calculated on the basis of induced coupled plasma emission analysis (ICP). During the preparation process, P123, starch, and silicon and zirconium can self-assemble, at temperatures and times of approximately 100 °C and 24 h. The reaction time is critical (less than or greater than 24 h) and higher temperatures appear poorly assembled or dreadful in the structure, reducing the surface area and the size of the pores.

2.2 Characterization

SZr-SMC sample was characterized by BET (Brunauer–Emmett–Teller, X-ray diffraction (XRD), scanning electron microscopy (SEM), transmission electron microscopy (TEM) X-ray photoelectron microscopy (XPS), programmed thermodesorption of ammonia (NH3-TPD) and FTIR of pyridine (Py). XRD results were acquired using a PANALITYCAL Phillips X'pert XDS diffractometer with a diffractometer beam monochromator and a CuKα radiation source. The BET surface area and pore size distribution of the material was analyzed by nitrogen adsorption using a surface area analyzer (Quantachrome/Autosorb1). Chemical states of the elements of sulfated-Zr-SMC identified by XPS acquired on a Microtech Multilb 3000 spectrometer, equipped with a hemispherical electron analyzer and MgKα ($h\nu = 1253.6$ eV) photon source. The surface morphology of the SMC was characterized by scanning electron microscopy performed in a JEOL JSM-6610LV Scanning with energy-dispersive X-ray spectroscopy (EDS). The acid properties by the ammonia-TPD, in a Micromeritics Chemisorb 2720 equipment. The samples were pretreated with N_2 at 400 °C for 3 h. Afterward, the sample was exposed to NH3 vapors for 45 min at ambient temperature. NH_3-TPD profiles were collected under He flow at 20 mL/min and a heating rate

of 10 °C/min from room temperature to 700 °C. The FTIR spectra were obtained from a JASCO 5300 Fourier Transform spectrometer. The pyridine adsorption and desorption studies were conducted in a vacuum line, evacuated at 10–4 Torr for 4 h, and heating at different temperatures. The samples (self-supported wafers), were first degassed at 400 °C for 1 h under vacuum, using a cell with CaF_2 windows.

2.3 Evaluation of catalytic activity

The SZr-SMC activity was evaluated in two processes: the catalytic decomposition of isopropanol was used as a test reaction for the study of the effective acidity or redox-active sites. A fixed bed tubular glass reactor working at atmospheric pressure was used for a solid charge of 35 mg without dilution (0.3–0.5 mm particle size). The sample was pretreated at 250 °C in an N_2 flow for 2 h (80 mL/min). Isopropanol was fed into the reactor by flowing N_2 (total flow of 40 mL/min with 30% isopropanol), analyzing the influence of the reaction temperature. The reaction products were analyzed by an on-line gas chromatograph provided with an FID and a fused silica capillary column. However, SZr-SMC activity was investigated in the gas phase alkylation of aniline with methanol at T °C = 300; Methanol/Aniline = 3 and different conversion levels, obtained by varying the contact time, (based on aniline w/f). The reaction system consisted of a fixed bed reactor constructed of 8 mm id 300 mm long Pyrex glass, placed in a controlled furnace using a cutting pyrometer. The reagents were introduced into the reaction zone employing a positional displacement pump. The reaction products were analyzed by gas chromatography, using a 30 m. long AT-WAX capillary column with temperature programming and FID detectors.

3 Results and discussions

3.1 The synthesis process

The principal variation of the synthesis technique concerning that reported by Wu et al. [22], which we mentioned the synthesis procedure, is that we include zirconium in the self-assembly system of the hydrolyzed TEOS, with the template (P123) and the carbon source (starch). In this way a different interaction between the reagent originates, which after the process described above, builds a material based on mesoporous carbon with zirconium in its structure, without the presence of zirconium oxide as a bulky species, as will be shown later. The template method is an efficient technique to synthesized mesoporous materials with characteristics specific such as a high surface area and pore-sized uniform within mesopores range. TEOS is used to control

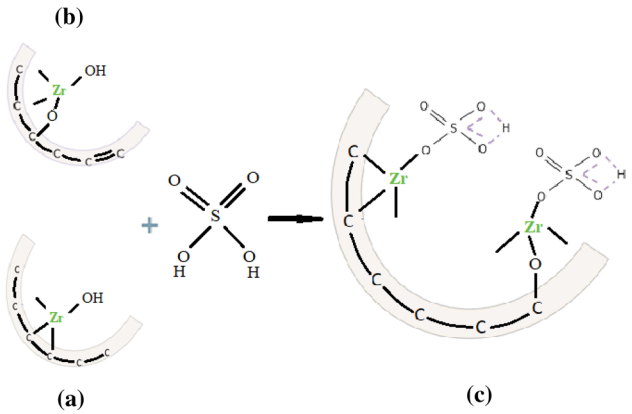

Scheme 1 Proposed interaction of mesoporous carbon walls with Zr: **a** Zr–C, **b** Zr–O–C; **c** monodentate Zr-sulfate superacid sites

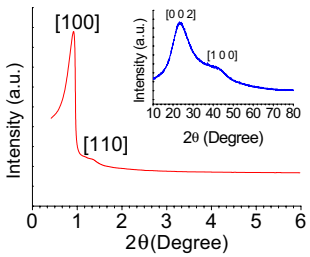

Fig. 1 Low-angle X-ray diffraction and inset at high-angle of SMC

the textures of both the P-123 and starch hydrolyzed; the silica source condenses around the composite formed between the template and carbon precursors. The incorporation of TEOS at synthesis reaction was made to obtain mesoporous carbons with tunable pore structure. The silicon source acts as a hard template to be able to maintain the shape of the carbon molecules in successive treatments that are conducted on the material, among them, the dehydration reaction in an acid medium (H_2SO_4) and calcination at high temperatures. Employing this method of simultaneous synthesis (sol–gel method), the pore structure of the carbonaceous material is precisely controlled. Scheme 1 shows possible active site formation on mesoporous carbon (SMC).

3.2 XRD-BET-TEM-EDS studies

Figure 1 shows the diffraction patterns of the SZr-SMC: at low-angle and inset at high-angle. At low-angles, the main signal around $2\theta = 0.9°$ corresponds to plane reflection (100), while the $2\theta \approx 1.4°$ is produced from plane reflection (110). The two reflection signals can be assignable to a hexagonal P6mm crystallographic space group [23]. The value of the spacing d was used to calculate the cell parameter a_0, considering that it is a hexagonal type unit cell, the values of $d_{100} = 10.69$ nm, and the cell parameter is 12.35 nm. The

cell parameter a_0 is considered to be the distance from center to center of the pores, with a well-defined arrangement of hexagonal or cylindrical channels of infinite length.

The inset Fig. 1 shows two broad signals at high angles, which can be indexed to the (002) and (100) planes typical of graphite carbons.

The material has many uniform macropores on its surface characteristics of mesoporous carbon (Fig. 2a). Figure 2b shows typical hysteresis loops with capillary condensation (P/Po > 0.55) of SZr-SMC and the pore size distribution (≅ 3.5 nm). The hysteresis loops correspond to isotherm type-IV, indicating a mesoporous structure.

The hysteresis loops show H3 characteristics, which can be attributed to slit-shaped pores. SZr-SMC has a large surface area of up to 1300 m^2/g, and a total pore volume of 0.94 cm^3/g (Fig. 2b) composed mainly of mesoporous with an average pore size of approximately 3.5 nm (Fig. 2c).

Elemental mapping of S by energy-dispersive X-ray spectroscopic (EDS) is shown in Fig. 2d. The presence of S–O or S=O bonds was indeed verified by XPS in the next section.

ZrO_2 crystals were not detected, indicating that the material has zirconia interacts with the walls of SMC, with the absence of clusters of metallic oxides dispersed on its surface, such as we corroborate with XRD and XPS studies (Fig. 3).

3.3 XPS studies

The surface composition and chemical states of the elements of sulfated-Zr-SMC (SZr-SMC) were studied using XPS (Fig. 3). The C 1s signals are shown in Fig. 3a, whose deconvolution helps us determine three modes of bonding the C. The first peak is assigned to C–C with sp^3 hybridization and the second with sp^2 hybridization typical of Carbon Graphite. The interesting aspect is to observe the energy binding attributed to the Zr–O–C link at 287.8 eV [24, 25], without presenting SZr-SMC material, C–OH bonds. In Fig. 3b, the species S–O or S=O that are attributed to sp^2 appear as a broad signal around 170 eV. Additionally, Zr signals ($3d_{5/2}$ and $3d_{3/2}$) located around 182.5 and 185.0 eV

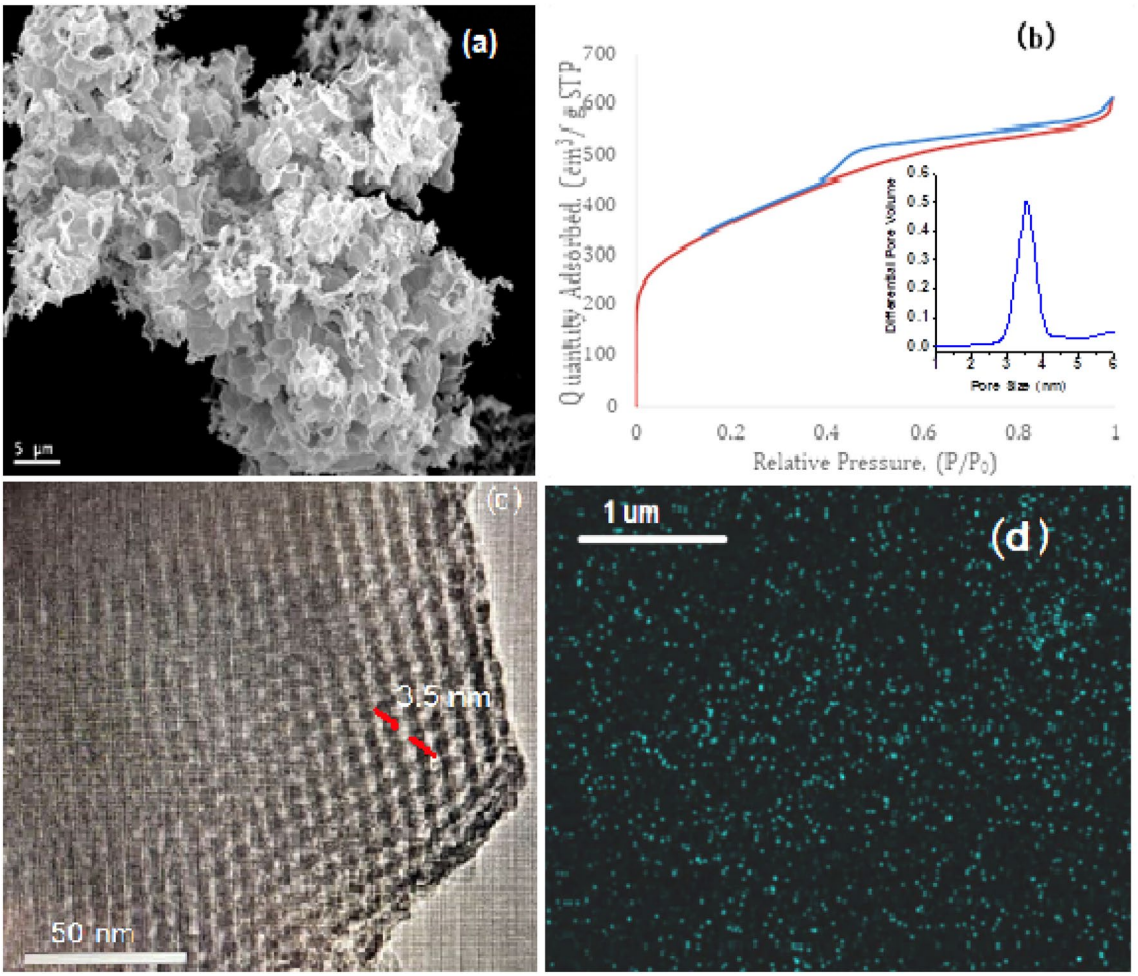

Fig. 2 SEM image (**a**), BET Isotherm and pore distribution (**b**), TEM (**c**) and EDS mapping of S (**d**), of SZr-SMC

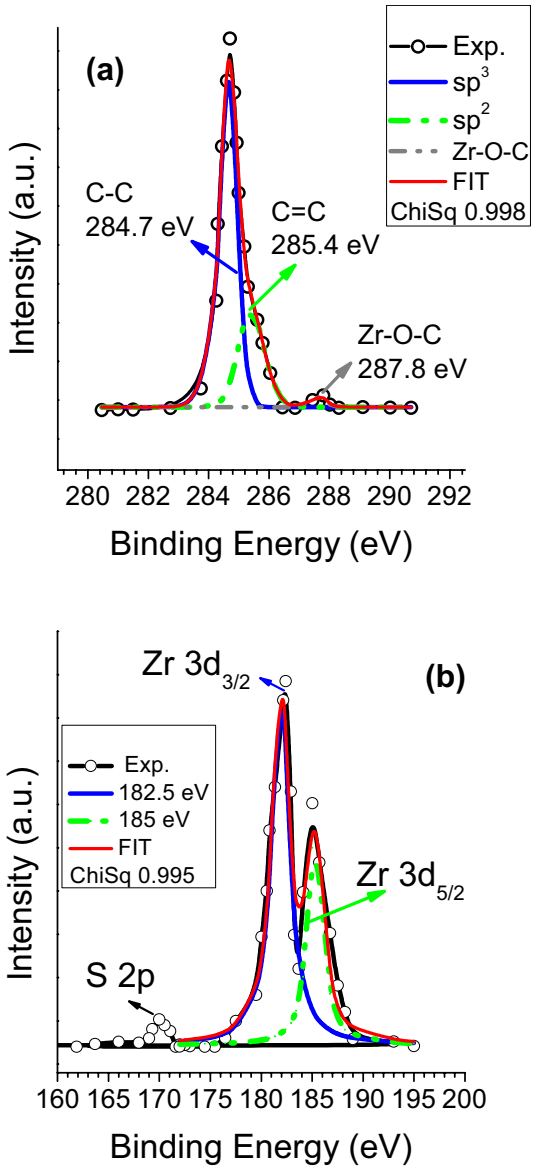

Fig. 3 XPS spectra of SMC, C 1s peak deconvolution (**a**), Zr 3d peak deconvolution (**b**) of SZr-SMC

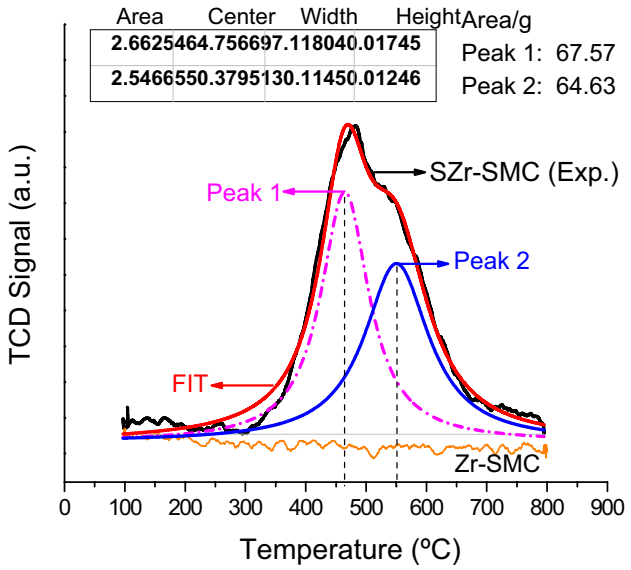

Fig. 4 NH_3-TPD of SZr-SMC and Zr-SMC

(±0.2) do not correspond to pure ZrO_2 [17, 26]. It can be deduced that the interaction of SO_4^{2-} and ZrO_2 decreases the electronic density in the Zr core displacing at higher binding energies the Zr signals in the XPS studies [27], indicating that a catalyst with attractive acidic properties was generated as shown below.

3.4 Ammonia TPD studies

In the ammonia-TPD studies (Fig. 4), we have taken special care to reduce the lag times in the sample cell and in the pores (large pore size) that tend to interfere with the process profiles, and therefore these effects were negligible. TPD models found in the literature deal with experiments conducted either under vacuum or under an inert gas stream. The theory previously exposed assumes that ammonia concentration gradients develop within the zeolite pores of the samples during the TPD runs [28]. Since we work under N_2 flow and larger pore sizes of mesoporous carbon, we suggest that this state is unaccountable for the occurrence of the TPD maxima observed in this work. However, free re-adsorption effectively occurs at pretreatment temperatures under 477 °C but desorption is irreversible above this temperature. In an excellent review Niwa and Katada [29], reported on the benefits and drawbacks of ammonia TPD. The total concentration of the acid sites and the concentration of their relative strength was determined by NH_3-TPD. Regarding the strength of acidic sites, some authors [30, 31], have reported that ammonia desorption signals below 400 °C correspond to sites with weak surface acidity, while desorption signals are exhibited at temperatures above 400 °C corresponding to sites with higher acidity. Sani et al. [32], showed NH_3-TPD profiles of the original ZSM-5, and it was reported that the modified catalysts SZr / ZSM-5 obtained a total of 3.71 and 0.75 mmol/g of ammonia retained, respectively (corresponding to desorption from 150 to 550 °C), with a maximum approximately 300 °C for parent ZSM-5 and 450 °C for sulfated zirconia containing-zeolite. Wu et al. [33], studied the acidity of ZSM-5 with varying Si/Al ratios by ammonia TPD, finding that all samples displayed two NH_3 desorption peaks. One of the peaks is located in the temperature range of 208–222 °C and the other one is in the range of 398–427 °C, which corresponds to a weak and strong acidic sites, respectively. H-ZSM-5(Si/Al = 30) presented the greatest density of sites, with a total acidity of

1.71 mmol/g, weak: 0.99, and strong 0.72 mmol/g. Das et al. [34], concluded that the low surface exposed when using mesoporous sulfated zirconia, might be the cause of the low total acidity 0.147 mmol/g, achieved by the NH_3-TPD profile, but with a high acidic strength at a maximum of 577 °C.

The NH_3-TPD results achieved in this work are shown in Fig. 4. Zr-SMC material does not retain ammonia, revealing the absence of acidity. The SZr-SMC catalytic material has a broad peak between 380 and 700 °C. The value with a maximum at 465 °C and another of approximately 550 °C was determined by deconvolution of the NH3-TPD profiles. The deconvolution area of the peaks has an experimental error of ± 5 area/g. As a function of the TPD study, there are 1.28 and 1.21 mmol/g of NH_3 retained (first and second Peak, respectively), corresponding to the moderate and strong acid sites. The total acidic sites are 2.49 mmol/g, greater than the number of Zr species (1.16 mmol/g), isolated and adhered to the catalyst surface.

This difference suggests the presence of Bronsted acid sites due to SO_4^{2-} species and Lewis acid sites due to zirconium species. In the graphite structure (our XRD studies indicate that SMC has typical graphite carbon planes), and by using XPS of the C 1s peak (Fig. 3a), it can be attributed to the hybridized carbon sp^3 and sp^2 and the Zr–O–C; the latter are the potential anchoring sites of sulfated Zr species in the walls of SMC. When the atomic S/Zr ratios are greater or around 1, as is our case 0.9 [35, 36], the existence of a monodentate structural species is suggested. It appears that the catalyst has more than one type of active site caused by more than one mode of interaction of Zr with the carbonaceous wall of the material.

3.5 FTIR studies

The FTIR results are shown in Fig. 5 and Table 1. The application of Fourier Transform Infrared Spectroscopy (FTIR) is widely known, in the determination of acid sites, using a base, mainly pyridine as a probe molecule [37]. Thus, in Fig. 5, we show the spectra of adsorbed pyridine (see experimental section), desorbed in a vacuum at various temperatures.

Emeis et al. [38], estimated the number of acidic sites from early and well-known studies. The criteria for assessing acidic sites as weak, medium and strong to those sites that retained Py (at 10^{-4} Torr), above 250, 350, and 450 °C, respectively, using H-ZSM-5, HZn-ZSM-5, and InH-BEA, has been reported by us [39, 40]. Among other authors [31, 32], similar criteria were adopted using H-ZSM-5 and SZr-ZSM-5. In this work, we apply as criteria to determine the Py evacuation temperatures, the values of the NH_3-TPD study profiles, despite the difference between the pKb of both bases. Thus, we start the evacuation at the temperature at which ammonia is observed, in the NH_3-TPD studies

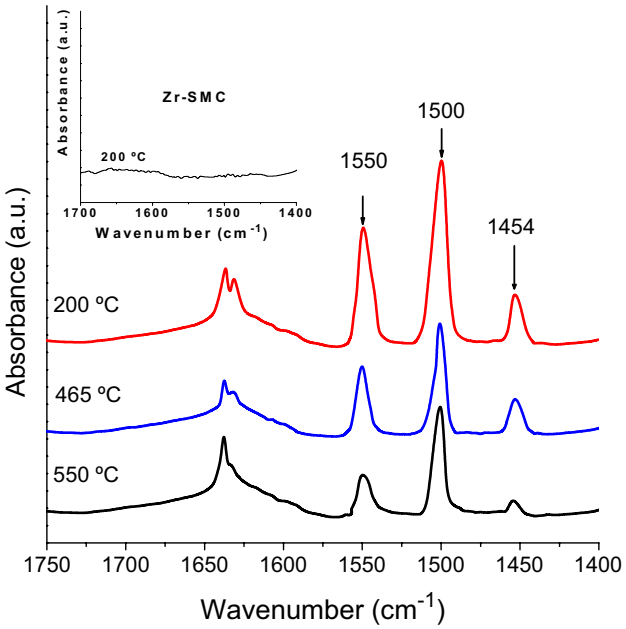

Fig. 5 FTIR of pyridine retained at different temperatures on SZr-SMC

(200 °C), to have the first idea of the total acid sites. The second premise was to evacuate at 465 °C and 550 °C (maximum of the first and second NH_3-TPD peaks, respectively).

Thus, knowing the total acid sites, we would arbitrarily infer the acid properties of the material in three categories: weak or medium acid sites (WMAS), strong acid sites (SAS) and super acid or super-strong sites (SSAS). The WMAS was calculated as the total Py retained after evacuation at 200 °C minus Py retained at 465 °C; the SAS as the total Py minus WMAS minus Py retained above 550 °C, and the SSAS sites as the quantity of Py retained at more than 550 °C (Table 1). This study allowed to differentiate Bronsted and Lewis sites for each case and to perform a qualitative and quantitative analysis of the acid properties of SZr-SMC. Figure 5 indicates that, as the desorption temperature of Py, pre-adsorbed on SZr-SMC, decreases the bands attributable to Bronsted acid sites (1550 cm^{-1}), Lewis acid sites (1454 cm^{-1}) and the band of approximately 1495 cm^{-1} typically assigned to a combined band related to Bronsted and Lewis sites [41]. Simultaneously, it can be observed that the retention of Py over 550 °C (SSAS) is a consequence of Bronsted acid sites, which are 3 times higher than Lewis acid sites, allowing as, a first approximation, to assume that the catalyst provides a more Bronsted SSAS. In addition, the inset in Fig. 5 appears in the same study conducted on the material before it was sulfated (Zr-SMC), and remarkably, but in line with the NH_3-TPD studies, it has no acid sites. Wen-Hua Chen et al. [42], found that pure ZrO_2 samples display only bands in association with the Lewis sites, while Bronsted sites appeared after its sulfation, which

Table 1 FTIR data of SZr-SMC acidic sites as a function of pyridine* retained at different temperatures

Desorption temp. °C	Py** (mmol/g)		Py** (mmol/g) for regions					
	BS	LS	WMAS		SAS		SSAS	
			BS	LS	BS	LS	BS	LS
200	1.37	0.99						
465	0.98	0.77						
550	0.43	0.18						
			0.25	0.17	0.75	0.58	0.43	0.18
Total	2.36		0.42		1.33		0.61	

*Before desorption at 10^{-4} Torr for 4 h

**$\pm$0.015 mmol/g

would once again substantiate the absence of ZrO_2 as bulky species in Zr-SMC and SZr-SMC material. Recently, Yunjie Wang [43], reported an interesting material based on zirconium oxide deposited on ordered silicon walls, and subsequently sulfated, named OMSZS and the proposed structure is $S_2O_8^{2-}/ZrO_2$-SiO_2. The material showed higher acidity, determined by FTIR of pre-adsorbed and desorbed pyridine at various temperatures, retaining it at 550 °C, mainly due to Lewis acid sites (1445 cm^{-1}), and in much lower proportion Bronsted sites, unlike from this work, using SZrSMC, in which the higher proportion is due to Bronsted sites. The superacidity is found only as a function of the retained pyridine adsorption on Lewis sites at desorption temperatures of 650 °C. Rivoira et al. [44], have reported only the occurrence of acidic Lewis sites in a Ce-Zr-SBA-15-based catalyst, suggesting its cause in the existence of Zr^{4+} isolated into the framework. The amount, nature and strength of acidic sites of the SZr-SMC catalytic material, acquired by FTIR of Pyridine are listed in Table 1.

According to Fig. 5, Zr-SMC materials have not retained pyridine from 200 °C in evacuation temperature. The data of Table 1 indicate that for each temperature range of evacuation, the number of Bronsted sites is slightly greater than Lewis, finding that above 550 °C, SZr-SMC has the most Bronsted sites. The total of acid sites, (that determined after evacuation to 200 °C and 10^{-4} Torr for 4 h, is approximately 2.36 mmol/g, slightly less than those obtained by NH_3-TPD (2.49 mmol/g) but greater than the number of Zr species (1.16 ± 0.05 mmol/g) content in the catalyst). According to the regionalization criteria of the acid strength, described, in WMAS, SAS and SSAS, we found that it was distributed in, 0.42, 1.33, and 0.61 mmol/g respectively, having in consideration that the implicit error is ± 0.015 mmol/g.

If we consider the sum of the SAS and SSAS regions, 82% of the sites are strong and only 18% are weak-medium. These results lead us to consider, in addition to the inhomogeneity of acid sites, the existence of at least two types of active species of sulfated Zr-SMC, responsible for distributing strength. The reason, for which we study in this work, the determination of acidity by both NH_3-TPD and pyridine FTIR methods, is related to the fact that several authors using similar catalysts have applied one or the other method and it is more difficult to compare the results. For example, recently, Tonutti et al. [45], examined the acidity of H-ZSM-5, reported a total of 1.4 mmol/g of total acid sites, between 25 and 727 °C, but used the temperature of desorption of pyridine, applying similar criteria from us, to the regional distribution of acidic strength. To assess the activity of the catalyst, two catalytic evaluations are presented below that corroborate the strength and nature of the sites determined by Py-FTIR.

4 Activity Studies

A wealth of information can be found on the determination of acidity (strength and nature) of ZrO_2, sulfated zirconia, sulfated zirconia supported in various materials, with micropores and mesoporous, and of various natures, either siliceous (the majority), alumina or carbonaceous supports, etc. Besides, there are many divergences (but very interestingly, when it comes to having a more comprehensive view of the problem), in the operating conditions that employ probe molecules, such as isomerization of *n*-pentane [46], butanes [47, 48], and 1-butene [49] to iso-derivatives of the products, and attributable to the type and strength of acidic sites. Sulfated mesoporous zirconia, which showed the presence of moderately good acid sites, was found to be highly active for the synthesis of biodiesel products based on long-chain fatty acids [50]. Aniline alkylation with methanol has also been used, trying to infer the existence or coexistence of Bronsted-Lewis acid sites, and isopropanol dehydration to determine even redox sites. These determinations have been made with several zirconia sulfate catalysts with a single common denominator, which is that the zirconia is found as an oxide, isolated and with sulfate deposited on the low exposed surface of zirconia, although the size of the

zirconia is reduced to 8 nm [51]. In this work, we do not observe, by either XRD, XPS, or TEM the presence of zirconia mass or bulky, which allows us to suggest that Zr should act as an atomic species and maintain its electronic properties (LUMO–HOMO), either in the self-assembly process with starch and Zr-SMC later formation, or in the sulfatation process. For the above reasons, we compared the activity of catalysts in the conversion of isopropanol with the results obtained by other authors, at the same reaction conditions. Moreover, we evaluated the activity of SZr-SMC for alkylation of aniline with methanol. Furthermore, we use the strategy of the optimum performance envelope technique (OPE), which is well-documented because it enables us to determine if the reaction products are primary, secondary, stable, or unstable. In this study it is especially useful since the distribution products are sensitive to the conversion level, which was obtained at a constant temperature, varying the catalyst mass/aniline flow ratio, in a piston flow reactor described in the experimental section.

4.1 Aniline alkylation with methanol

In previous works, in search of the generation of polyaniline within-host channels such as, MCM-41, SBA-15 [52], SBA-3 and SBA-16 [53], (whose weak acidity was demonstrated), we studied aniline adsorption by infrared spectroscopy. We observed that aniline is adsorbed in large proportion by the SBA hosts, through the π electron system of the aniline, with electron acceptor sites of this material, i.e. the Si–OH groups, leaving free amine groups, which allowed its subsequent PANI polymerization. Thus, in this case, the catalysts with weak acid sites can interact with the aniline similarly giving free amine groups to be alkylated. However, if the acid sites are strong or super acid, the interaction with aniline is through the NH_2– group, leaving the aromatic ring of the aniline free for its potential alkylation.

Surprisingly (Fig. 6), when we studied the alkylation of aniline with methanol, a comparative analysis of all reaction products obtained indicates that:

- Toluidine is the initial and stable product of aniline alkylation with methanol, with the highest yield and more than 95% selectivity in all ranges of aniline conversion.
- *N*-methylaniline (NMA), is primary an unstable product, reaching only at 1.7 mol% at aniline conversion of 42 mol%
- *N*,*N*-dimethylaniline (NNDMA), is derived from NMA alkylation, so it is a secondary stable reaction product, reaching 2.29 to 72 mol% aniline conversion.

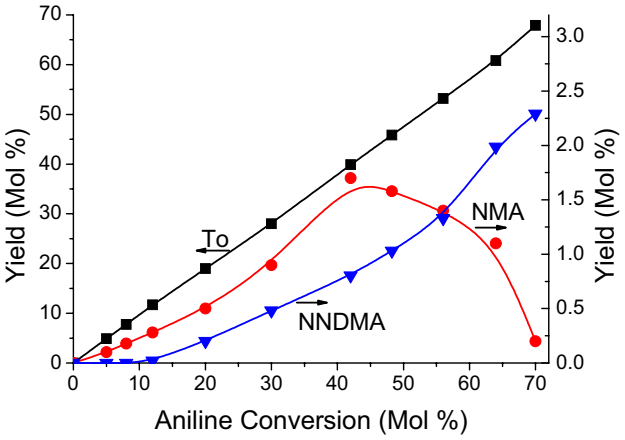

Fig. 6 OPE curves of SZr-SMC: activities (product yields) versus Aniline conversion, extrapolated at zero time and at 380 °C

- 2,4-Dimethylaniline (DMA), 2,3,4-trimethylaniline (TMA), was not produced.

These results corroborate the new SZr-SMC catalytic material mainly offers sites of strong and very strong acidity. Thus, Toluidine appears as the main product in the entire range of aniline conversions. Furthermore, Fig. 6 significantly demonstrates how the low alkylation levels of the amino groups generate low production of NMA and NNDMA [54, 55]. Results are in correlation with TPD and FTIR analysis, and the low proportion of ammonia or pyridine retained below 465 °C, which can be considered to denote medium or weak acid sites, which are active for the alkylation of the NH_2– group of aniline.

The recyclability and stability characteristics of this type of catalysts are essential, especially when used in the aniline alkylation reaction with methanol. For this reason, we selected the operating conditions at which the highest aniline conversion was achieved according to the data in Fig. 6 at T °C = 380; Methanol/Aniline = 3, and 10 min time on stream time (fresh sample). Thus, Fig. 7 shows the results of aniline conversion and toluidine production of the fresh sample and after 5 cycles of 4 h each. Up to the third cycle, no catalyst deactivation is observed, after which both aniline conversion and toluidine yield decrease. Then, after the fourth cycle, the catalyst was calcined at 550 °C in static air during 5 h, and recovered in the fifth cycle its high conversion (> 69%) and toluidine production (> 67%) as obtained with the fresh catalyst. This phenomenon demonstrated that calcination had a positive impact on the recovery of catalytic activity, as the active sites of the catalyst were "cleaned" by removing adsorbed organic species (coke formation). As a result, the recyclability and reusability of the catalyst without loss of activity was effectively determined. Furthermore, according to ICP studies of S and Zr of the reactivated material, the

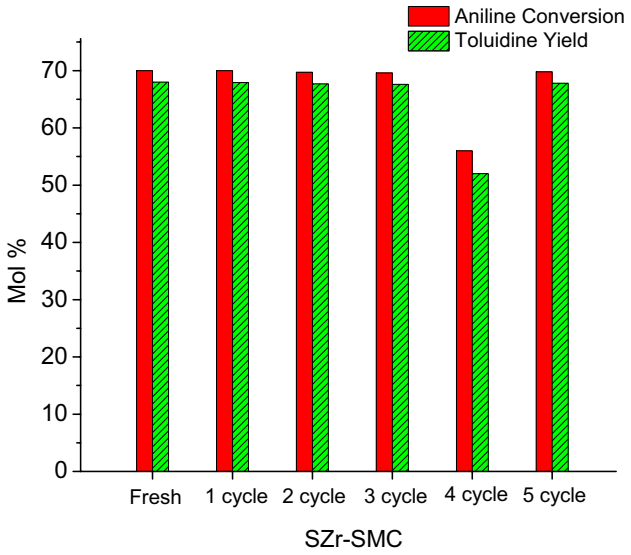

Fig. 7 Catalytic activity of SZr-SMC after five catalytic cycles. T = 380 °C, aniline/methanol = 3; cycle reaction time = 4 h

chemical composition was not affected (2.38 ± 0.05 mmol/g of Zr and a ratio S/Zr of 0.987), similar for the pristine sample. Concerning the effect of the re-activation process on the availability of acid sites, additional pyridine adsorption and desorption studies at 550 °C revealed 0.425 and 0.182 mmol/g corresponding to SB and SL respectively, similar to the reported concentrations for the fresh sample (Table 1).

4.2 Isopropanol conversion

Using the isopropanol conversion reaction, the catalysts can be categorized according to their acidity in dehydration or dehydrogenation to propene or acetone, respectively. Dehydration of isopropanol to propene occurs in acidic sites, while dehydrogenation to acetone is performed in redox or basic sites. The catalytic characteristics of Al-SBA-15 for dehydrating isopropanol were studied by us, showing that the acidic sites are only the active sites within the mesostructure of H-Al-SBA-15 [56], in agreement with the weak acid sites of Al-SBA. Different authors employed this reaction using ZrO_2-based catalysts on different supports, finding also that the presence of redox sites was due to the bulky oxide [54–56]. Table 2 illustrates the catalytic activity of SZr-SMC at various temperatures. Alvaro Reyes-Carmona et al. [50], employing sulfated zirconium oxide supported on silica SBA-15 evaluates it in the catalytic tests of isopropanol dehydration and 1-butene isomerization. A good catalyst with strong acid sites was identified, with the sample with 20 wt% of ZrO_2 as the best performer. SBA-15 was not active in the conversion of isopropanol. Between other catalysts, the highest efficiency catalyst, as indicated by the

Table 2 SZr-SMC activity to isopropanol conversion at different temperatures and TOS

Catalyst	Temperature (°C)			
	Conversion/selectivity (mol%)[a]			
	125	175	200	250
SZr-SMC/TOS[b]				
1	55/100	70/100	90/100	100/100
5			90/100	100/100
10			90/100	100/100
15			89.9/100	99.7/100
20			89.9/100	99.7/100
H-Al-SBA-15 (Ref. [56])	25/100	65/100	80/100	–
SZ20S (Ref. [50])	–	20/100	42/100	–
MCMSiZr7	–	–	40/100	–
MSUSiZr7 (Ref. [57])	–	–	90/100	

[a]Selectivity to propylene, ± 0.5%

[b]Time on stream (TOS), h

(Ref. [56]) H-Al-SBA-15

(Ref. [50]) SZ20S (Si/Zr = 20) sulfated

(Ref. [57]) SiZr7: zirconium doped MCM; MSU (Si/Z r = 7)

author, was ZrO_2-SBA-15 sulfated with 20% ZrO_2-substrate, analyzed from 150, 175 and 200 °C reaching at 13, 21, and 42% of Isopropanol conversion level and 100% selectivity for propylene, with traces of diisopropyl ether only at 200 °C. Fuentes-Perujo et al. [57], using the Si-MCM-41, deduced that the acidity of the siliceous solids was low, meanwhile, the incorporation of Zr(IV) in the siliceous structure caused an increment in acidity. The Brønsted sites are linked with bridged Zr–OH and Zr–O (H)–Si groups. The Lewis acid sites diminish in intensity by temperature but are still found at 350 °C. Hence, these zirconium-doped solid shows Lewis acid sites. Isopropanol conversion at 400 °C was 30% and the selectivity to propylene and acetone was 80% and 20%, respectively, on Si-MCM-41 [57]. Moreover, on MCM-Zr at 200 °C, the conversion was 40% and the selectivity to propylene was 100%. The evaluation of the acidity of MSU in the conversion of isopropanol showed that it was inactive for the reaction, while MSU with various Zr doped content (MSU-SiZr), in general, showed 90% selectivity to propylene at 200 °C [57]. As expected, catalytic materials based on mesoporous silica are inactive for the conversion of isopropanol, in line with its acid strength. The incorporation of Al as a heteroatom or the deposition of sulfated ZrO_2 on these siliceous supports increases their acidity and activity for the reaction. According to the data in Table 2, the high activity of SZr-SMC material for the conversion of isopropanol and the high selectivity to propylene can be noted. Moreover, at

low temperatures, the conversion levels are elevated compared to the data of the literature [50, 55–57], but per the presence of SAS and SSAS determined by FTIR of pyridine. In the whole temperature range studied, neither acetone nor diisopropyl ether was detected. The Zr-SMC material shows a low conversion even at high temperatures (3% at 350 °C), as expected from the lack of available acidic sites.

As can be seen in Table 2, the activity and stability in the conversion of 2-propanol to propylene was compared with a silica structure with Al as lattice heteroatom, and with to Si_3–O–Al–OH type acid sites in Al-SBA-15 [56], the same silica structure (SBA-15) but doped with ZrO_2-sulfate as active sites [50, 56]. Another silica structure, with Zr in a mesoporous silica structure [57]. Whatever the type of active site and the support, the acidic SZr-SMC material synthesized in this work, is more active in the conversion of 2-propanol to propylene. We suggest that the reason for these differences is related to the superacid nature of the active sites of the material. Furthermore, in all cases, the conversion is a function of increasing reaction temperature.

Table 2 also shows that the SZr-SMC catalyst maintained its catalytic activity toward propylene production (studying the reusability effect at temperatures of 200 and 250 °C) after four cycles of 5 h duration each (time on stream, TOS), without additional activation, thus reaching a total of 20 h of continuous reaction. These results indicate the absence of irreversible adsorption of both the reagent and product, and the possible polymerization leading to carbon deposition blocking the access pores to the material, as well as the permanence of the active species.

Two Langmuir–Hinshellwood mechanisms were considered (using the gas–solid reaction, at atmospheric pressure in a fixed-bed microreactor), assuming that the surface reaction is likely that both mechanisms occur simultaneously [58], an E1 (two steps, carbocation formation and then propylene), and E2 (one step, propylene as the only species formed by intramolecular dehydration).

Lamier et al. [59], using alumina as a catalyst, reported that in both cases (E1 or E2 mechanism), the reaction temperature is found to be the key parameter in 2-propanol conversion, and tailoring the alkene/ether selectivity, rather than morphology influences, which in turn strongly affect the amount of active sites and thus the catalytic activity. Otherwise, the two mechanisms have similar activation energy (~ 98 kJ/mol), with an exothermic adsorption–desorption heat, which makes if the active site is strongly Bronsted, the conversion of 2-propanol increases with temperature, due to the modest decrease in activation energy (~ 10 kJ/mol), for the step involving the loss of water from the adsorbed reactant on acidified matrices [60]. This decrease in activation energy with temperature is associated with an easier loss of water from the protonated alcohol molecule through a concerted mechanism, yielding higher 2-propanol conversion.

When the active sites are sulfated zirconium ($SZrO_2$), as the Zr content increases [61], its dehydrogenation activity produces acetone.

5 Nature of SZr–C interaction

Having reached this point in our work, and considering in addition to the studies already shown, which indicate the absence of ZrO_2 clusters, complementary UV–Vis diffuse reflectance experiments of SZr-SMC showed no absorption bands around 230 and 290 nm attributable to isolated ZrO_2, neither as monomers nor as oligomers, respectively [62, 63], we must ask ourselves a question to which we will try suggesting two answers.

According to Wu et al. [22], synthesized by auto-assembly of hydrolyzed TEOS, P123 and starch, a carbonaceous material after oxidation with sulfuric acid, indicates, the possibility of competition between hydrolyzed TEOS and P123 and the OH groups of starch, generating a hybrid material of Si–C, that then when extracting the silicon, generates SMC, with the presence of –OH stretching vibration sites determined by FTIR. The material does not have zirconium. At this point, the first difference from our SZr-SMC is that we do no detect acid sites before sulfation. On the other hand, Ziyuan Zhao [60], used the technique of interstitial carburation to manufacture carbide coatings for zirconium. The coatings showed a microstructure gradient with a volume ratio of ZrC to 100%, and adhesion among the coating and the base was strong, but the material was achieved at more than 1150 °C obtaining high-carbon steel and zirconium sheet. To do so, a novel self-template technique is suggested to synthesize ZrO_2 (5–10 nm) nanoparticles embedded in carbon (ZrO_2/C). It offers clear evidence for understanding the catalytic synergy of ZrO_2 and C provides a new approach for preparing encapsulated carbon metal oxides, with efficient catalytic activity and with light metals as hydrogen storage materials. XRD data confirm that it has been successful in synthesizing ultrafine ZrO_2/C and ZrO_2 nanoparticles.

An alternative to the question, about Zr–C interaction, without the presence of ZrO_2, is a model involving two acid sites for each monodentate species according to our suggestions from the NH_3-TPD and Py-FTIR results, where the total acid content was higher than that of the zirconium species in the catalyst. Therefore, the SZr-SMC catalyst has strong Lewis and Bronsted acid sites [61]. In the simplest linear systems π, bonding to metals occurs by two interactions. The density of the electrons is donated directly to the metal, as a σ bond would be formed. Also, the Zr^{4+} can donate electron density back to the linear system π C=C of the orbital d of the metal to the orbital π* empty of C=C of SMC [64], see Scheme 1a.

Amin Osatiashtiani [65], studied by XANES, the interactions of ZrO_2 on SBA-15 and SZr-SBA-15, arriving in the fact that the tetragonal ZrO_2 contains two not equivalent tetrahedral ZrO_4 units, with different lengths of Zr–O linkage, either in sulfated or non-sulfated materials. The load sharing of the local Zr surroundings is awaited to follow its covalent union to the SO_4^{2-} assemblies.

A signal at 287.8 eV attributed to Zr–O–C was detected by XPS [22, 24]. We suggest that Zr–O–C bonds could be related to the large amount of -OH groups in the carbon source (starch), which would facilitate the formation of such bonds and incorporate Zr into the carbonaceous network. Wu et al. [22], found HO–C sites, in their work on SMC-sulfate syntheses, although without the incorporation of Zr. Hence, since we did not find acidity in the Zr-SMC material, the proton found by Wu [22], have been replaced by us with Zr. SZr-SMC material should exhibit the nature and strength of specific acidic sites. Based on the aforementioned, we can suggest the second type of Zr-wall mesoporous carbon interaction of the SMC, as C–C–O–Zr (Scheme 1b). Both types of Zr–C and Zr–O–C interactions would conduce to the same type of sulfated site, the monodentate type (Scheme 1c). The sulfation of zirconia would cause the subsequent changes in surface acidity, concerning Bronsted acidity, generating a new type of Bronsted acid site, with the possibility of protons creating multicentric links with sulfate anions [66], and the electron acceptation properties of Zr are potentiated by the inductive power of the SO_4^{2-} anion, which would withdraw the electron density from Zr or by its direct activation with the O atom of the sulfate complex.

6 Conclusion

We have presented a novel synthesis procedure for the formation of solid acid catalysts consisting of SMC functionalized with sulfated zirconia. During the crystallization process, P123, starch, zirconia and silicon can be co-assembled. After the sulfuric treatments, the physical characteristics of the parent carbon were maintained in the final material, showing a large surface area (1300 m^2/g), a large pore volume and a well-ordered porosity composed of uniform mesoporous of approximately 3.5 nm. XRD, SEM, TEM and XPS studies indicated the absence of ZrO_2 as a bulky species. Thus, Zr as an isolated species was successfully anchored in the SMC for subsequent sulfation. Besides, evidence from XPS C 1s data can be attributed to the hybridized carbon sp^2 (from the graphitic structure of mesoporous carbon), which would form Zr–C bonds. Moreover, the large amount of –OH groups, from the starch used as a carbon source, would promote the formation of Zr–O–C species (also detected by XPS), forming part of the walls of SMC, in the self-assembly process. The evidence of two high-temperature desorption peaks in the NH_3-TPD profile and the high pyridine retention temperature determined by FTIR revealed medium, strong and super-strong acid sites on the SZr-SMC catalyst, and it can be assumed that these sites correspond to a superacid catalyst. Catalytic evaluations in the alkylation of aniline with methanol and the selective conversion of isopropanol to propylene, confirm the acidic properties of the SZr-SMC material.

Acknowledgements OAA, MLM CONICET researchers, UTN-FRC. The authors thank FONCyT. PICT 2017-2021, Nº 1740.

References

1. J. Liu, N.P. Wickramaratne, S.Z. Qiao, J. Mietek, Nat. Mater. **14**, 763 (2015)
2. A.H. Jadhav, H. Kim, I.T. Hwang, Catal. Commun. **21**, 96 (2012)
3. X. Qi, M. Watanabe, T.M. Aida, L. Smith, Catal. Commun. **10**, 1771 (2009)
4. R. Kourieh, V. Rakic, S. Bennici, A. Auroux, Catal. Commun. **30**, 5 (2013)
5. M.H. Tucker, A.J. Crisci, B.N. Wigington, N. Phadke, R. Alamillo, J. Zhang, S.L. Scott, J. Dumesic, ACS Catal. **2**, 1865 (2012)
6. T. Yamaguchi, K. Tanabe, Y.C. Kung, Mater. Chem. Phys. **16**, 67 (1987)
7. A. Song, S. Xuemin, A. Sayari, Catal. Rev. Sci. Eng. **38**, 329 (1998)
8. H.K. Mishra, A.K. Dalai, D.D. Das, K.M. Parida, N.C. Pradhan, J. Colloid. Interface. Sci. **272**, 378 (2004)
9. M.H. Zong, Z.Q. Duan, W.Y. Lou, T.J. Smith, H. Wu, Green Chem. **9**, 434 (2007)
10. W.Y. Lou, M.H. Zong, Z.Q. Duan, Bioresour. Technol. **99**, 8752 (2008)
11. S. Suganuma, K. Nakajima, M. Kitano, D. Yamaguchi, H. Kato, S. Hayashi, M. Hara, J. Am. Chem. Soc. **130**, 12787 (2008)
12. M. Okamura, A. Takagaki, M. Toda, J.N. Kondo, T. Tatsumi, K. Domen, M. Hara, S. Hayashi, Chem. Mater. **18**, 3039 (2006)
13. M. Godino-Ojer, L. Milla-Diez, I. Matos, C.J. Durán-Valle, M. Bernardo, I.M. Fonseca, E Pérez Mayoral. Chem. Cat. Chem. **10**, 5215 (2018)
14. V. Budarin, J.M. Clark, J.J.E. Hardy, R. Luque, K. Milkowski, S.J. Tavener, A.J. Ashley, Angew. Chem. **118**, 3866 (2006)
15. K. Milkowski, J.H. Clark, Green Chem. **6**(4), 189 (2004)
16. S. Doi, J.H. Clark, D.J. Macquarrie, K. Milkowski, Chem. Commun. 2632 (2002)
17. J.C. Juan, Y. Jiang, X. Meng, W. Cao, M.A. Yarmo, J. Zhang, Mat. Res. Bull. **42**, 1278 (2007)
18. D.-J. Guo, X.-P. Qiu, W.-T. Zhu, L. Quan, Appl. Catal. B Env. **89**, 597 (2009)
19. X. Wan, L. Yuchen, X. Huining, P. Yuanfeng, L. Jie, RSC Adv. **10**, 2932 (2020)
20. Z. Tan, H. Xiao, R. Zhang, Z. Zhang, S. Kaliaguine, New Carbon Mater. **24**(4), 333 (2009)
21. A. Mftah, F.H. Alhassan, M.S. Al-Qubaisi, M.E. El Zowalaty, T.J. Webster, M. Sh-eldin, R. Abdullah, Y.H. Taufiq-Yap, S.S. Rashid, Int. J. Nanomed. **10**, 765 (2015)
22. M. Wu, P. Ai, M. Tan, B. Jiang, Y. Li, J. Zheng, W. Wu, Z. Li, Q. Zhang, X. He, Chem. Eng. J. **245**, 166 (2014)
23. M.R. Anantharaman, E. Veena Gopalan, K.A. Malini, G. Santhosh Kumar, T.N. Narayanan, P.A. Joy, I.A. Al-Omari, Y. Yasuhiko, D. Sakthi Kumar, Nanoscale Res. Lett. **5**, 889 (2010)

24. P. Dhanasekaran, R. Sharon, S.R. Williams, D. Kalpana, S.D. Bhat, RSC Adv. **8**, 472 (2018)
25. P. Dhanasekaran, S.V. Selvagenesh, S.D. Bhat, New J. Chem. **41**, 13012 (2017)
26. C. Morterra, G. Cerrato, S. Ardizzone, C.L. Bianchi, M. Signoretto, F. Pinna, Phys. Chem. Chem. Phys. **4**, 3136 (2002)
27. Y. Ou, W. Tsen, S.C. Jang, F.S. Chuang, J. Wang, H. Liu, S. Wen, C. Gong, Electrochim. Acta **264**, 251 (2018)
28. R.J. Gorte, J. Catal. **75**, 164 (1982)
29. M. Niwa, N. Katada, Chem. Rec. **13**, 432 (2013)
30. A. Corma, Chem. Rev. **97**, 2373 (1997)
31. M. Turco, J. Catal. **117**(2), 355 (1989)
32. Y.M. Sani, P.A. Alaba, A.O. Raji-Yahya, A.R. Abdul Aziz, W.M. Ashri, W. Daud, J. Taiwan Inst. Chem. Eng. **60**, 247 (2016)
33. G. Wu, W. Wu, X. Wang, W. Zan, W. Wang, C. Li, Microp. Mesop. Mater. **180**, 187 (2013)
34. S.K. Das, M.K. Bhunia, A.K. Sinha, A. Bhaumik, J. Phys. Chem. C **113**, 8918 (2009)
35. K.H. Chung, S. Jeong, H. Kim, S. Kim, Y.K. Park, S.C. Jung, Catalysts **7**, 321 (2017)
36. R. Akkari, A. Ghorbel, N. Essayem, F. Figueras, Appl. Catal. **328**, 43 (2007)
37. T. Barzetti, E. Selli, D. Moscotti, L. Forni, J. Chem. Soc. Faraday Trans. **92**, 1401 (1992)
38. C.A. Emeis, J. Catal. **141**, 347 (1993)
39. O.A. Anunziata, G. Gonzalez Mercado, Catal. Lett. **107**(1–2), 111 (2006)
40. O.A. Anunziata, A.R. Beltramone, E.J. Lede, F.G. Requejo, J. Mol. Catal. A: Chem. **267**, 272 (2007)
41. F. Babou, G. Coudurier, J.C. Vedrine, J. Catal. **152**, 341 (1995)
42. W.-H. Chen, H.-S. Ko, A. Sakthivel, S.-J. Huang, S.-H. Liu, A.-Y. Lo, T.-C. Tsai, S.-B. Liu, Catal. Today **116**, 111 (2006)
43. Y. Wang, H. Yuan, Z. Zhang, Y. Ke, J. Porous Mater. **27**, 429 (2020)
44. L.P. Rivoira, V.A. Valles, M.L. Martínez, Y. Sa-ngasaeng, S. Jongpatiwut, A.R. Beltramone, Catal. Today **360**, 116 (2021)
45. L.G. Tonutti, H.P. Decolatti, C.A. Querini, B.O. Dalla Costa, Microp. Mesop. Mater. **305**, 110284 (2020)
46. G. Zhu, C. Wang, Y. Zhang, N. Guo, Y. Zhao, R. Wang, S. Qiu, Y. Wei, R.H. Baughman, Chem. Eur. J. **10**, 4750 (2004)
47. Y. Sun, S. Ma, Y. Du, L. Yuan, S. Wang, J. Yang, F. Dengv, F.-S. Xiao, J. Phys. Chem. B **109**, 2567 (2005)
48. B. Banerjee, S. Bhunia, A. Bhaumik, Appl. Catal. A: Gen. **502**, 380 (2015)
49. G.V. Echevskii, D.G. Aksenov, E.G. Kodenev, E.V. Ovchinnikova, V.A. Chumachenko, Petrol. Chem. **59**, 101 (2019)
50. A. Reyes-Carmona, R. Moreno-Tost, J. Mérida-Robles, J. Santamaría-González, P.J. Maireles-Torres, A. Jiménez-López, E. Moretti, M. Lenarda, E. Rodríguez-Castellón, Adsorption **17**, 527 (2011)
51. P. Madkikar, X. Wang, T. Mittermeier, A.M. Videla, C. Denk, S. Specchia, H.A. Gasteiger, M. Piana, J. Nanostruct. Chem. **7**, 133 (2017)
52. O.A. Anunziata, M.B. Gomez Costa, M.L. Martinez, Catal. Today **133**, 897 (2008)
53. M.L. Martinez, F.A. Luna D'Amicis, A.R. Beltramone, M.B. Gomez Costa, O.A. Anunziata, Mater. Res. Bull. **46**, 1011 (2011)
54. L. Jiang, F. Guo, Y. Wang, J. Jiang, Y. Duan, Z. Hou, Asian J. Org. Chem. **8**, 2046 (2019)
55. S. Moulay, Curr. Org. Chem. **23**, 1695 (2019)
56. O.A. Anunziata, A.R. Beltramone, M.L. Martínez, L. López Belon, J. Colloid Interface Sci. **315**, 184 (2007)
57. D. Fuentes-Perujo, J. Santamarıa-Gonzalez, J. Merida-Robles, E. Rodrıguez-Castellon, A. Jimenez-Lopez, P. Maireles-Torres, R. Moreno-Tost, R. Mariscal, J. Solid State Chem. **179**, 2182 (2006)
58. J. Bedia, R. Ruiz-Rosas, J. Rodríguez-Mirasol, T. Cordero, J. Catal. **271**, 33 (2010)
59. K. Larmier, C. Chizallet, N. Cadran, S. Maury, J. Abboud, A.F. Lamic-Humblot, E. Marceau, H. Lauron-Pernot, ACS Catal. **5**, 4423 (2015)
60. V.E. Diyuk, L.N. Grishchenko, V.K. Yatsimirskii, Theor. Exp. Chem. **44**(5), 331 (2008)
61. Y. Tang, E. Zong, H. Wan, Z. Xu, S. Zheng, D. Zhu, Microp. Mesop. Mat. **155**, 192 (2012)
62. Y. Du, S. Liu, Y. Zhang, F. Nawaz, Y. Ji, F.S. Xiao, Microp. Mesop. Mat. **121**, 185 (2009)
63. A. Infantes-Molina, J. Mérida-Robles, P. Maireles-Torresa, E. Finocchio, G. Busca, E. Rodríguez-Castellón, J.L.G. Fierro, A. Jiménez-López, Microp. Mesop. Mater. **75**, 23 (2004)
64. Z. Zhao, F. Liu, Q. Wang, J. Li, L. Zhong, Y. Xu, P. Hui, J. Zhu, F. Yan, M. Zhao, J. Alloys Compd. **834**, 155110 (2020)
65. A. Osatiashtiani, A.F. Lee, M. Granollers, D. Brown, L. Olivi, G. Morales, J.A. Melero, K. Wilson, ACS Catal. **5**, 4345 (2015)
66. L.M. Kustov, V.B. Kazansky, F. Figueras, D. Tichit, J. Catal. **150**, 143 (1994)